China Ocean Eng., 2019, Vol. 33, No. 5, P. 573–582
DOI: 10.1007/s13344-019-0055-z, ISSN 0890-5487
http://www.chinaoceanengin.cn/ E-mail: coe@nhri.cn

A Numerical and Experimental Study on the Hull-Propeller Interaction of A Long Range Autonomous Underwater Vehicle

WANG Ya-xing[a, c, *], LIU Jin-fu[a, c], LIU Tie-jun[a, c], JIANG Zhi-bin[a, c], TANG Yuan-gui[a, c], HUANG Cheng[b]

[a]State key Laboratory of Robotics, Shenyang Institute of Automation, Chinese Academy of Sciences, Shenyang 110016, China

[b]Wuchang Shipbuilding Industry Group Co., Ltd., Wuhan 430060, China

[c]Institutes for Robotics and Intelligent Manufacturing, Chinese Academy of Sciences, Shenyang 110016, China

Received October 4, 2018; revised May 5, 2019; accepted June 4, 2019

Abstract

Range is an important factor to the design of autonomous underwater vehicles (AUVs), while drag reduction efforts are pursued, the investigation of body-propeller interaction is another vital consideration. We present a numerical and experimental study of the hull-propeller interaction for deeply submerged underwater vehicles, using a proportional-integral- derivative (PID) controller method to estimate self-propulsion point in CFD environment. The hydrodynamic performance of hull and propeller at the balance state when the AUV sails at a fixed depth is investigated, using steady RANS solver of Star-CCM+. The proposed steady RANS solver takes only hours to reach a reasonable solution. It is more time efficient than unsteady simulations which takes days or weeks, as well as huge consumption of computing resources. Explorer 1000, a long range AUV developed by Shenyang Institute of Automation, Chinese Academy of Sciences, was studied as an object, and self-propulsion point, thrust deduction, wake fraction and hull efficiency were analyzed by using the proposed RANS method. Behind-hull performance of the selected propeller MAU4-40, as well as the hull-propeller interaction, was obtained from the computed hydrodynamic forces. The numerical results are in good qualitative and quantitative agreement with the experimental results obtained in the Qiandao Lake of Zhejiang province, China.

Key words: underwater vehicle, hydrodynamics, hull-propeller interaction, RANS simulation

Citation: Wang, Y. X., Liu, J. F., Liu, T. J., Jiang, Z. B., Tang, Y. G., Huang, C., 2019. A numerical and experimental study on the hull-propeller interaction of a long range autonomous underwater vehicle. China Ocean Eng., 33(5): 573–582, doi: 10.1007/s13344-019-0055-z

1 Introduction

As demands for autonomous underwater vehicles (AUVs) are becoming more and more challenging and complex, AUVs are supposed to be faster, be operated for longer range and be more maneuverable than ever before. The requirement for energy efficiency in design and operation of AUVs has been continuously increasing over recent decades. For AUV designers and researchers, one fundamental is about correctly estimating the resistance and self-propulsion performance for different operating cases. As reviewed for hydrodynamics of naval architecture and ocean engineering by Stern et al. (2015), computational fluid dynamics (CFD) continue to develop at ever-faster speed. It is showing inevitable potential to change engineering design from build-and-test design process to simulation based design approach, which will improve safety while saving cost. CFD codes are also widely used for the optimization and estimation of propeller-hull interaction of underwater vehicles.

Open water performance of propellers have been studied and experimentally tested for more than two hundred years since it was invented. Towing tank tests were widely adopted to investigate open water performance and wake variation of propellers under various loads (Denny, 1968; Di Felice et al., 2009, Felli et al., 2011). As numerical technique developed, both potential flow and CFD approaches became popular for propeller design and optimization. Potential flow method is easier to develop and use, but it is reliable only when limited viscous effects need to be considered (Young and Kinnas, 2003). According to the com-

Foundation item: This work was financially supported by the National Natural Science Foundation of China (Grant No. 41806122), the Strategic Priority Research Program of the Chinese Academy of Sciences (Grant No. XDA11040102), the State Key Laboratory of Robotics of China (Grant No. 2017-Z08), Youth Innovation Promotion Association, CAS, and Jiang Xinsong Innovation Fund.

*Corresponding author. E-mail: wangyaxing@sia.cn

parison of open water performance obtained from the potential flow Panel code and Reynolds averaged Navier−Stokes (RANS) solver by Gatchell et al. (2011), potential flow methods only gave reasonable results when the advance ratio is higher than 1.3. CFD method has higher accurate than potential flow approaches and lower cost than tank tests, and many works were carried out to capture wake and transient effects of propellers by CFD codes. Some of these researches include Martínez-Calle et al. (2002), Rhee and Joshi (2005), Califano and Steen (2011) and Morgut and Nobile (2012). These works prove that CFD approach can predict torque and thrust in good agreement with experiment test results. Besides routine simulation, CFD method may also be applied to research on special operating conditions of propellers (Martio et al., 2017).

For the prediction of hydrodynamic performance of propellers, there are also different specific techniques such as sliding mesh (Shen et al., 2016), overset mesh (Shen et al., 2015), steady moving reference frame (MRF) (Bhattacharyya et al., 2016) and actuator disk (Kim et al., 2018). When sliding mesh and overset mesh techniques simulate actual rotation of propellers, their only difference is the way dealing with the interface between rotating and non-rotating mesh domains. As unsteady solver is needed for the simulation, and to capture features of the flow around propellers, very small time step has to be used, and this dramatically increases the computational burden. MRF and actuator disk methods are compromise proposals to reduce CPU time. Actuator disk method can produce thrust and torque on the base of the known propeller performance curves, it is practicable but not accurate. MRF is a good solution to mimic the effect of a constant rotation without actually moving the vertices of mesh, and a steady solution without the necessary of a transient method is required. This is a simplification and time-efficient approach for prediction of hydrodynamic performance of propellers.

When being fixed in the stern region of ships or AUVs, action of propellers may lead to a significant difference in the pressure field on the hull body. Because it is restricted by measurement technique, factors for assessment of hull-propeller interaction cannot be evaluated according to in-service data only (Hobson et al., 2012). CFD method is also widely applied in this field. Works by Phillips et al. (2009), Ueno and Tsukada (2016), Dubbioso et al. (2017), Hayati et al. (2013) prove that the effect of the hull-propeller interaction should not be neglected, but these approaches still need a large amount of time-consuming computations. To date, CFD methods have been used to assess the hydrodynamic performance of propeller in the presence of an AUV or ship hull. Carrica developed a method to perform self-propulsion computations of surface ships (Carrica et al., 2010) and underwater vehicles (Chase and Carrica, 2013), even performance near surface in calm water and waves corresponding to a sea state 5 (Carrica et al., 2018), in which the propeller is gridded as an overset object, and a speed controller is used to adjust its rotational velocity to figure out the self-propulsion point. Sezen et al. (2018) estimated self-propulsion characteristics of DARPA SUBOFF with E1619 propeller. Besides self-propulsion simulations, some numerical test basins can also be used to study hull-propeller interaction. Coe (2013) developed an unsteady RANS simulation method that in conjunction with a 6-DoF rigid-body kinematic model to conduct AUV maneuvering simulations. Other works by Wang et al. (2018) and Guo et al. (2018) also made great contribution to the study of hull-propeller interaction of ships. Besides numerical simulations, experiments were also carried out as benchmark and validation of CFD predictions for deeply submerged manoeuvring performance, as well as concept studies. Experiments by Overpelt et al. (2015) were widely referenced to proceed further research for validation of manoeuvring simulations.

As remarkable as numerical simulation development is, to date, the obtained technology for assessment of hull-propeller interaction is still a time and resource consuming process. If unsteady simulation method is used, it may take days or weeks to evaluate propeller performance even using supercomputers. An efficient approach to figure out hull-propeller interaction of underwater vehicles is proposed in this paper. Self-propulsion point, thrust deduction, wake fraction and hull efficiency can be easily estimated while accuracy is guaranteed. Explorer 1000, a long range AUV developed by Shenyang Institute of Automation, Chinese Academy of Sciences, with a MAU4-40 series propeller fixed at its rear was studied in detail by using both numerical and experimental methods.

The paper is organized as follows. Section 2 gives a brief introduction of Explorer 1000 AUV, whose experimental data were used to validate the proposed approach. Section 3 describes the simulation strategy used in this paper. Section 4 presents experimental and numerical study on the open water performance of the MAU4-40 propeller. Section 5 introduces the proposed simulation method in detail, and gives a comprehensive assessment on the hull-propeller interaction of Explorer 1000.

2 Explorer 1000 AUV

Explorer 1000 AUV shown in Fig. 1 is 6.5 m long, displaces 1.2 m^3 of water and has a dry weight of 1160 kg. The vehicle has been designed for ocean observation with high endurance and long range operations. It is supposed to meet the 800 m depth rating and two weeks endurance. The cruising speed is 2 kn, and the maximum speed is 5 kn. To achieve maximum range, the angle of attack of vehicle can remain close to zero with the help of adjustable buoyancy, which is produced by two high-precision variable buoyance systems. The system advantages lie in three aspects: two-way adjustable with high accuracy and efficiency, and arranged fore and aft separately offers convenience to control

Fig. 1. Explorer 1000 AUV.

Fig. 2. MAU4-40 propeller.

pitch angle. After launch, the system generates negative buoyance and constant pitch angle to dive with limited energy consumption. When it closes to target depth, the system works again to reach a balanced condition. When ship moves at a fixed depth, both angle of attack and control surfaces will be near zero to save energy.

The hull of Explorer 1000 is a typical body of revolution with long middle-cylindrical form, which is a favorite option for AUV designs. The ratio of the hull length to diameter is about 12, which produces better stability rather than maneuverability. Owing to the necessary of communication, measurement and recovery, some appendages are fixed along the hull, and they generally amplify the unsteady features of the flow and deteriorate hydrodynamic performance of vehicles.

Hull-propeller interaction is a key component of endurance; after hull and appendages are decided at detailed design stage, propeller is designed. Besides requirement of cruising and maximum speed, it should also fit to speed-torque characteristic curve of motor to achieve an overall high power efficiency. According to the principle of propeller design by atlas method, propeller is designed on the basis of MAU4-40 series, a well-known series in marine industry. According to the design result, a four-blade propeller is designed as shown in Fig. 2, whose diameter is 0.300 m, area ratio is 0.40, and hub-diameter ratio is 0.23. As the vehicle works in large depth with low speed, cavitation influence is unnecessary to consider.

3 Numerical simulation

The numerical simulation results presented in this paper were produced using STAR-CCM+, a prominent commercial CFD package. Reynolds averaged Navier−Stokes (RANS) approach is used to predict flows around vehicle and propeller because its computational cost is lower than those of large eddy simulation (LES) and detached eddy simulation (DES). "$k-\omega$ shear stress transport" ($k-\omega$ SST) turbulence model introduced by Menter (1994) was adopted for the numerical simulations due to good results obtained in our previous researches (Gao et al., 2016) and some other literatures in this field of study (de Barros and Dantas, 2012). It is also because this turbulence model provides good prediction of vortices distribution around vehicles (Phillips et al., 2010).

Research in this paper includes three types of cases to simulate: open water characteristics of MAU4-40 propeller, drag variation of vehicle hull and self-propulsion of underwater vehicle. Unstructured trimmed mesh was employed to generate grid, since it can generate 3D mesh containing a predominantly hexahedral mesh with minimal skewed cell. For regions where vortices and flow separation occur, users can define refinement according to how intensively the flow is disturbed, and mesh size increases from vehicle surface to outer boundaries. This offers a robust and efficient approach to generate high quality mesh for complex geometries or flows.

For the mesh near the hull and propeller external surface, enhanced wall treatment, a chosen turbulence model, is used to correctly model the viscous sublayer in the boundary layer. A function of non-dimensional wall distance y^+, which is the representative of the local Reynolds number, is defined as:

$$y^+ = \frac{\Delta y \rho \mu_\tau}{\mu} = \frac{\Delta y}{v}\sqrt{\frac{\tau_\omega}{\rho}}, \tag{1}$$

where Δy is the distance of the first layer from the body surface; ρ is the water density; μ_τ is the friction velocity; μ and v are the dynamic and kinematic viscosity coefficient, respectively; τ_ω is the shear stress at the body surface. For the enhanced wall treatment, the value of y^+ should be as close to one as possible. For this research, we adopted the All-y^+ treatments as our previous work (Gao et al., 2018). Its accuracy and robustness have been proven by good agreement between experimental data and simulation results.

4 Propeller in open water

4.1 Numerical simulation

The open water characteristics of propellers can be described with principal parameters defined as:

$$J=\frac{V_a}{nD}, K_T=\frac{T}{\rho n^2 D^4}, K_Q=\frac{Q}{\rho n^2 D^5}, \eta_0=\frac{K_T}{K_Q}\cdot\frac{J}{2\pi}, \quad (2)$$

where J, K_T, K_Q, and η_0 represent the advance ratio, thrust coefficient, torque coefficient and propeller hydrodynamic efficiency, respectively; V_a is the average inflow to propeller; ρ is the density of the fluid; n is the propeller rotational velocity; D is the propeller diameter; T and Q are the thrust and torque generated by propeller at open water test. For open water test, the Reynolds number is defined as:

$$Re=C_{0.75}\left[V_a^2+(0.75\pi\cdot n\cdot D)^2\right]^{1/2}\Big/\nu, \quad (3)$$

where $C_{0.75}$ is the chord length of blade at the position of $0.75D$. According to the advice by ITTC, Reynolds number for open water test should be about 3.0×10^5.

CFD simulation using the steady RANS solver of Star-CCM+ forms the present investigation of performance of propeller. Different from the towing tank test, propeller and shaft do not move forward, instead, constant inlet velocities are specified parallel to the propeller axial direction. The steady Moving Reference Frame (MRF) method is applied to simulate the propeller rotation. Fig. 3 shows the boundaries and mesh regions in the computational domain for open water performance prediction. It is composed of two regions, a static region where stationary with respect to the lab reference frame is applied, and a rotating region where the propeller rotation is defined by the MRF technique.

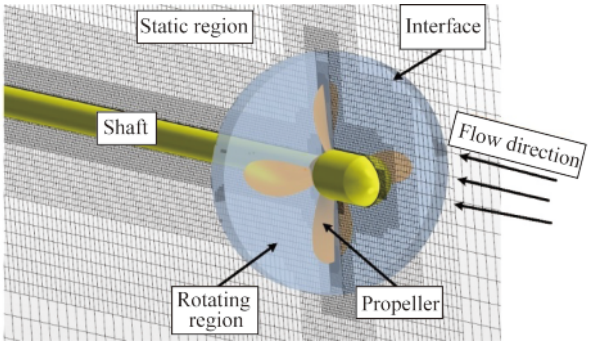

Fig. 3. Computational domain boundaries and mesh regions for open water prediction.

4.2 Open water test and validation

Towing tank test was conducted to evaluate the reliability of the selected simulation strategy and the open water performance of the designed MAU4-40 propeller. The towing tank is 150 m in length, 4.5 m in depth and 7.0 m in width. The propeller was fixed 0.5 m below the water surface. A standard test procedure with an ITTC propeller was first conducted to make sure all measuring instruments function normal. For values of advance ratio whose corresponding hydrodynamic efficiency is smaller than the maximum value, the relative error for K_T and K_Q should not be larger than ±1%. The rotational velocity of the propeller shaft was set to 720 rpm (revolutions per minute) throughout the tank test, and the towing velocity was changed between 1.5 m/s and 3.3 m/s to get different values of advance ratio. To eliminate the shaft impact on open water performance of propeller, a bare hub without blades was first fixed onto the shaft to conduct the test, axial force and torque were measured and recorded, and then propellers with blades were arranged and tested. The difference between without-blade test and with-blade test is thrust and torque generated by propeller rotation. The test procedure is shown in Fig. 4.

(a) Propeller test without blades (b) Propeller test with blades

Fig. 4. Test of open water performance of the MAU4-40 propeller.

CFD simulation follows the same procedure as towing tank test. Fig. 5 shows the open water performance (thrust coefficient, torque coefficient and efficiency) evaluated by Star-CCM+ compared with the towing tank test results for the MAU4-40 propeller. Good agreement can be concluded except for the efficiency when the advance ratio is large. This is expected due to the influence of smaller thrust coefficients. For Explorer 1000 AUV, according to previous design, its advance ratio is between 0.6 and 0.7. In this range, the average margin of error for efficiency, thrust and torque coefficients are about 6.8%, 6.2% and 1.2%, respectively.

5 Self-propulsion performance assessment

Two types of simulations of Explorer 1000 AUV were

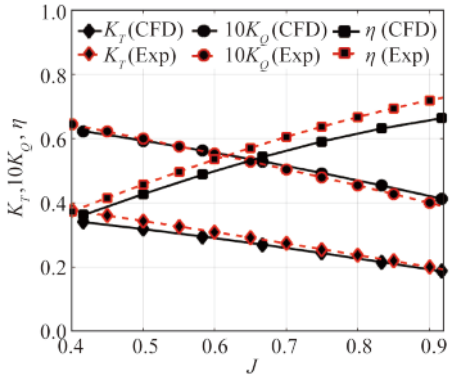

Fig. 5. Comparison between CFD and EFD results for the MAU4-40 propeller.

performed using Star-CCM+ and the methodology described in Gao et al. (2018). One type is AUV-only simulations at diverse angles of attack, and the other type is simulations of the AUV fitted with the MAU4-40 propeller under self-propelled conditions at diverse angles of attack. Self-propulsion points for different conditions were figured out with the help of the PID controller.

5.1 AUV-only simulation

In order to figure out the hull-propeller interaction of the AUV (Explorer 1000), The total drag of it has been firstly computed by CFD for both arrangements with and without nose appendages, which are named Layout01 and Layout02, respectively. The drag analyses have been carried out for different velocities as well as angles of attack from 0° to 3°. Drag coefficient is defined as:

$$C_{\mathrm{d}} = \frac{R_{\mathrm{h}}}{\frac{1}{2}\rho l^2 V^2}, \tag{4}$$

where R_{h} is the hull total drag without propeller behind, l is the hull length and V is the upstream velocity. Fig. 6 illustrates drag coefficients of Layout01 and Layout02 for different upstream velocities and angles of attack. It is evident that drag coefficients generally decrease as the upstream velocity increases, and the tendency is more obvious when the angle of attack is large. For Layout02, when the angle of attack is 3°, drag coefficients dropped by 8.2% as the upstream velocity changes from 3 kn to 5 kn, and the corresponding percentage for Layout02 is 4.4%. It is also noticeable that drag coefficients for upstream velocities of 3 kn and 4 kn are the largest when the angle of attack is 2°, but for 5 kn, the AUV experiences more resistance when the angle of attack is 0°, and the least when 3°. The only difference between Layout01 and Layout02 is that three appendages (Fig. 7), whose sizes are very small compared with the hull, are removed from Explorer 1000. This change makes the total drag drop by approximately 7.4%. The drop further verifies our previous research (Wang et al., 2019) that appendages fixed in the front of AUV make more contribution to the total drag than the others. Although drag coefficients decline with velocity increment, the gradient of changing is unpredictable especially when the angle of attack is small. This is mainly due to the fact that the total drag does not change much in those cases, as well as the variation of pressure drag is unpredictable.

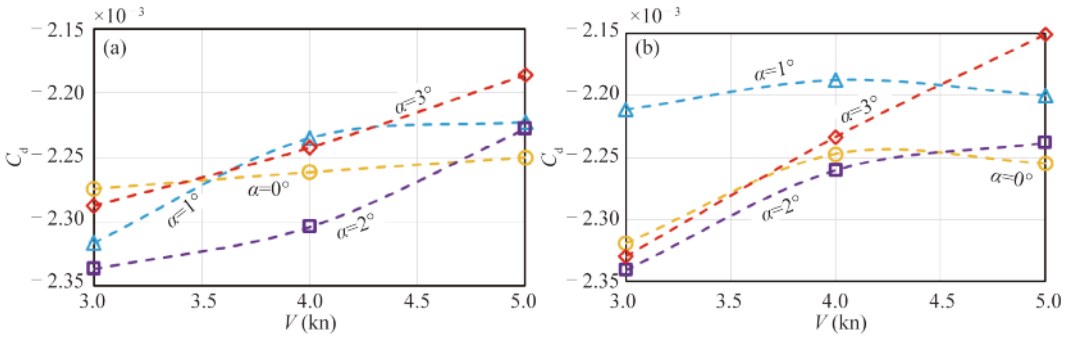

Fig. 6. Drag coefficients of Layout01 (a) and Layout02 (b) for different upstream velocities.

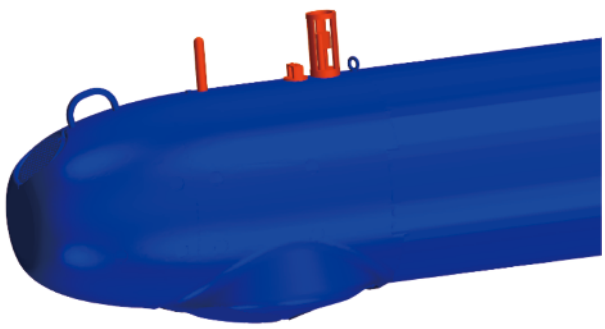

Fig. 7. Layout02 without the three marked appendages fixed on it.

5.2 Self-propulsion simulation

Different from previous works by Chase and Carrica (2013), Shen et al. (2015) and Phillips (2010), to figure out self-propulsion point for Explorer 1000 AUV at different velocity, an embedded controller was developed in the simulation platform to adjust rotational velocity. Proportional-integral-derivative (PID) was adopted because of its usability. The PID control system, as shown in Fig. 8, adjusts rotational velocity according to the deviation between resistance from water and thrust generated by propeller. The control law can be written as:

$$u(t) = K_{\mathrm{P}} e(t) + K_{\mathrm{i}} \int_0^t e(t')\,\mathrm{d}t' + K_{\mathrm{d}} \frac{\mathrm{d}e(t)}{\mathrm{d}t}, \tag{5}$$

where K_{P}, K_{i}, and K_{d} are coefficients for the proportional, integral and derivative terms, respectively. Proportional part K_{p} adjusts the controller linearly according to the difference between the desired set point $r(t)$ and current measured variable $y(t)$, the integral part K_{i} is in charge of eliminating the residual error by adding a control factor due to the historic cumulative value of the error, and the derivative part K_{d} estimates the future trend of the error according to its current rate of change.

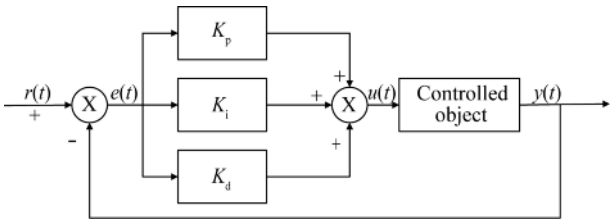

Fig. 8. PID control system.

For the rotational velocity control system, integral and derivative parts cannot be calculated directly. They need to be discretization handled as:

$$t = kT;$$

$$\int_0^t e(t')\,\mathrm{d}t' \approx T\sum_{j=0}^{k} e(j);$$

$$\frac{\mathrm{d}e(t)}{\mathrm{d}t} \approx \frac{e(k)-e(k-1)}{T}, \tag{6}$$

where T is the sampling period. The variation of rotational velocity and total drag during the procedure of finding self-propulsion point with the developed controller is shown in Fig. 9. Although steady flow equations are used to conduct simulations, oscillation of total force can be detected thanks to the propeller rotation defined by moving reference frames and the hull-propeller interaction. The rotational velocity fluctuates around a particular value while the monitored total hydrodynamic force averages around zero, which means a relative balance between hull resistance and propeller thrust.

The total grid number of the self-propulsion simulation is up to 10.5 million cells. The behind-hull flow distribution in velocity magnitude when simulation reaches a comparatively convergent state is shown in Fig. 10. Significant turbulence can be detected at the locations closed to the rotating propeller, but the intensity weakens obviously with distance increase.

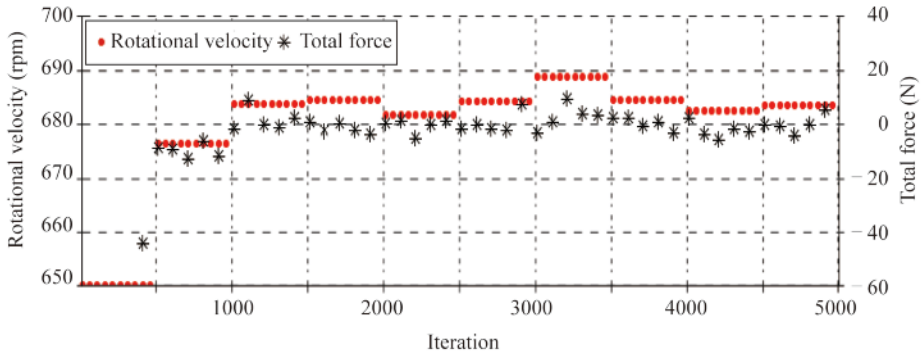

Fig. 9. Procedure of finding self-propulsion point (V=5 kn, θ=0°).

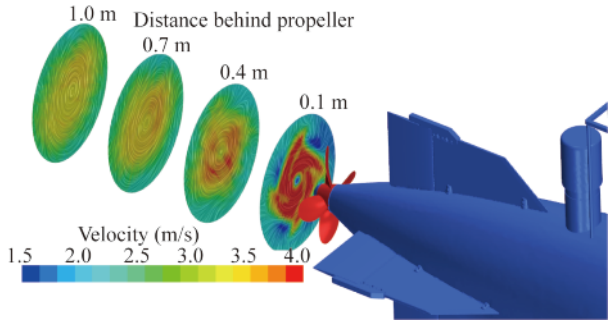

Fig. 10. Behind-hull flow distribution at the comparatively convergent state (V=5 kn, θ=0°).

5.3 Experimental data

Some trials for the two layouts mentioned in Section 5.1 were carried out in the Qiandao Lake of China's Zhejiang province to obtain some in-service data, so that the hull-propeller interaction of Explorer 1000 could be evaluated and validated. Three independent controllers were designed to make the AUV sail straight forward 10 m below the surface. The depth kept the minimum vertical forces and pitching moments due to the free surface. The three controllers were in charge of controlling forward speed, depth and orientation, respectively. The AUV was controlled to sail with depth and orientation unchanged at forward speed varying from 2 kn to 5 kn. Fig. 11 shows the variation of Layout01 in terms of forward velocity and pitch angle, both of them kept oscillating around particular value when the AUV

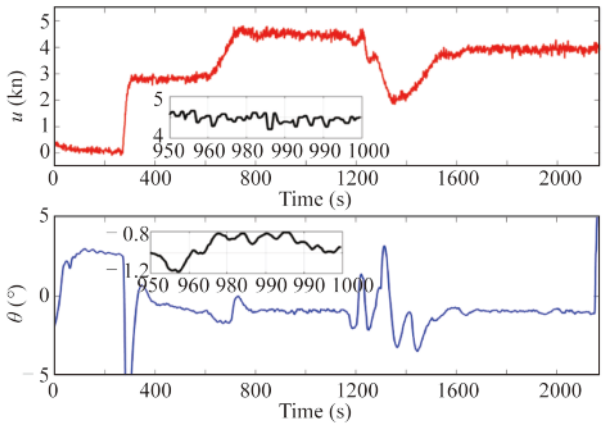

Fig. 11. In-service data of Explorer 1000 AUV.

reached a target status. The control precision of the forward velocity was about ±0.3 m/s, while that of the pitch angle was approximately ±0.2°.

5.4 Behind-hull performance

To achieve the expected speed and range, the in-service resistance of AUV and behind-hull performance of propeller need to be fully considered. For the in-service resistance, its components can be broken down into bare hull drag, appendage drag and induced drag. Bare hull drag is a basic component that can be obtained from towing tank test or numerical simulation; appendage drag adds both to the pressure drag and skin friction, for different AUVs, appendages lead to different level increase in resistance. Various instruments, aerials, etc., will also have associated impacts on total resistance, and induced drag is a consequence for an AUV to maintain its depth, because when keeping depth, AUV has to use control surfaces to reach a nose down flying condition to counteract a net positive buoyancy, which is an insurance to ensure AUV back to the surface in the event of a failure. Another contribution for drag increment is behind-hull rotation of propeller, which modifies the flow at the tail of the AUV while generating thrust to self-propulsion.

5.4.1 *Self-propulsion point*

When the target velocity, depth and orientation keep unchanged, after the adjusting stage, the AUV will come to a relatively stable state as shown in the subplot of Fig. 11. All parameters, including control inputs like control surfaces and propeller rotational velocity, as well as the monitored values of velocity, depth and orientation will fluctuate around a constant value in small range. The method adopted in this paper could not take the fluctuation into consideration, but multiple simulations for different angles of attack from 0° to 3° were carried out, and the PID controller introduced in section 5.2 was used to figure out their self-propulsion points. The comparison between simulations and trial data for Layout01 and Layout02 can be found in Fig. 12. For all simulations of the two layouts, the calculated propeller rotational velocities all were smaller than the average values from lake trials due to the ignorance of parameter fluctuations in lake trials. It can also be found that for the case V = 3 kn, the AUV experiences smaller propeller rotational velocity when the angle of attack is close to 1°, as for the case V = 5 kn, it will be better if the angle of attack is 0°. This is because that the pressure drag makes more contribution to the total drag than skin friction when the velocity is higher.

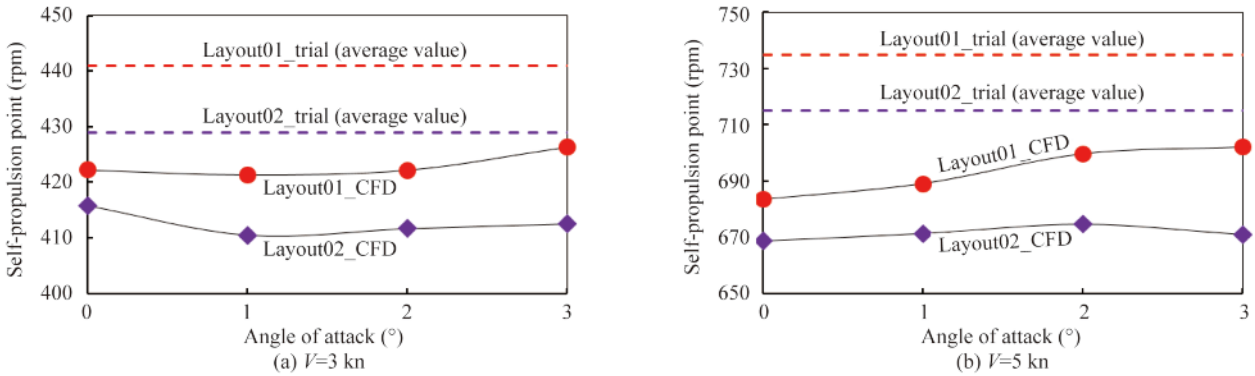

Fig. 12. Propeller rotational velocities under self-propulsion conditions for different angles of attack and different forward speeds.

Fig. 13 shows changes in the propeller rotational velocity for different velocities according to CFD simulations and lake trials. The CFD results were obtained from cases whose angle of attack was set to 1°. It is significant that propeller rotational velocity is nearly proportional to the velocity of the AUV because the drag of the AUV is theoretically equal to the thrust from the propeller when the balanced state without linear acceleration is reached, the advance ratio J for all velocities should be the same. The average errors between CFD simulations and lake trials are approximately 5%, which is acceptable for engineering application. According to the comparison between the two layouts, the removal of the three appendages at the nose makes the rotational velocity drop by around 2.7%, which saves about 7.3% of energy consumption consequently.

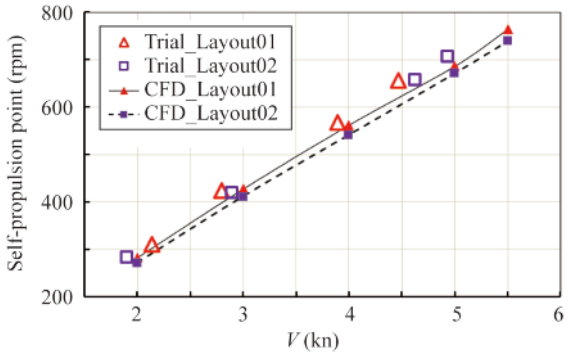

Fig. 13. Comparison of propeller rotational velocities between simulation results and data from lake trials for different layouts and forward velocities with the angle of attack being 1°.

5.4.2 *Thrust deduction*

Reduction of the local pressure in turn increases the pressure drag acting on AUV hull. The increase, also defined as thrust deduction factor t, can be written as:

$$t = 1 - \frac{R_h}{T_B}, \tag{7}$$

where T_B is the thrust generated by propeller when rotating behind hull. Pressure distribution on the surface of the AUV cannot be monitored from lake trials, but can be obtained with the help of CFD simulation. Fig. 14 shows changes in pressure variation along one of the AUV's longitudinal sections for different cases at the constant forward speed of 3 kn. For all those cases, pressure distributions between 0.1 and 0.8 of the total length are almost the same, which means that propeller rotation and angle of attack have no impact on this part at the balanced state. There are slight differences at the nose part among cases due to the effect of the angle of attack, but no distinction can be found whether the propeller is fixed behind the body of the AUV. Significant reduction of the local pressure can be found from 0.8 of the total length to the end, especially for the case the angle of attack is 3°. High fluctuation of pressure can be found at the rear of the AUV, which means that the larger angle of attack generates more vortexes, and plays negative effect on propeller thrust, because fluctuating input velocity leads to higher dissipation of energy.

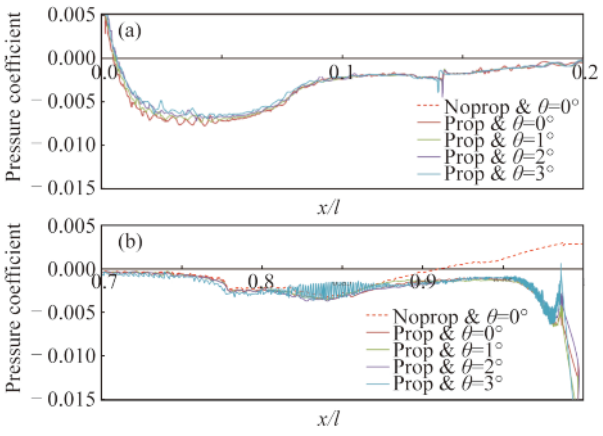

Fig. 14. Pressure distribution along hull nose (a) and tail (b) for the AUV with and without propeller, as well as different angles of attack.

With the help of numerical simulation, thrust from propeller fixed behind the AUV, as well as hull total drag without propeller behind, can be monitored, and the thrust deduction factors can be consequently calculated. The results are shown in Fig. 15. For all cases, the thrust deduction factors fluctuat between 0.15 and 0.22, and the average value is around 0.18. Smaller angle of attack tends to obtain smaller hull-propeller interaction. However, a relatively better performance can be found when the angle of attack is 2°,

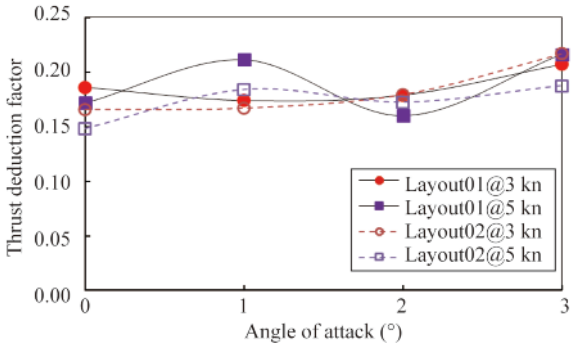

Fig. 15. Thrust deduction factor for different angles of attack.

compared with the value of 1°. This indicates that a detailed investigation should be conducted to improve the overall performance of underwater vehicles.

5.4.3 *Wake fraction*

When AUVs sail forward at certain speed, water close to hull surface is disturbed to generate wake behind their tail. This makes the average velocity of water flow into propeller smaller than the velocity of AUVs. This phenomenon consequently makes propellers generate less thrust than expected. Wake fraction ω, a dimensionless coefficient for the wake field strength, is used to evaluate the behind-hull performance of propellers. It is an essential consideration when designing a propeller for AUVs, and is defined as:

$$\omega = 1 - \frac{V_a}{V}, \tag{8}$$

where V_a is the actual inlet velocity to the propeller. V_a cannot be monitored from CFD simulation directly. But it can be obtained with the help of open water curves as shown in Fig. 5. For each case, thrust generated by the rotation of propeller is firstly calculated from CFD simulation which reaches a balanced state. Thrust coefficient K_T can be obtained as water density, propeller rotational velocity and propeller diameter are known. Its corresponding advance ratio J is calculated by easy curve fitting. The advance ratio helps get the actual inlet velocity V_a in the end. The variation of wake fractions for all cases can be seen in Fig. 16. Most wake fractions fluctuated between 0.3 and 0.37, with an average value of 0.35. When the angle of attack is 1°, wake fraction changes in a very limited range for all velocities and layouts, while that of the attack angle of 3° varies greatly. It indicates that the propeller experiences the most stable inlet flow when the angle of attack is 1°, contrast to 3° of the worst.

5.4.4 *Hull efficiency*

Hull efficiency η_H, the ratio of effective power to propeller thrust power, can be expressed as:

$$\eta_H = \frac{1-t}{1-\omega}. \tag{9}$$

It actually is not the efficiency in meaning of techno-

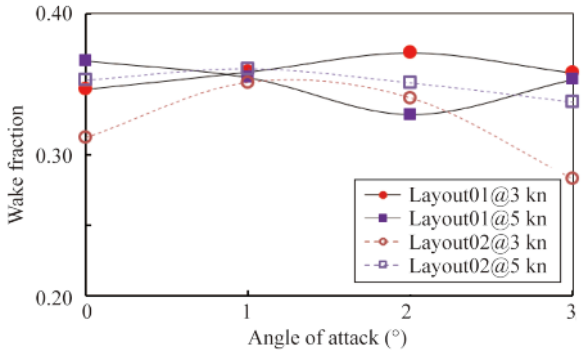

Fig. 16. Wake fraction for different angles of attack.

logy. It is rather the value that evaluates the influence of hull-propeller interaction on the efficiency of propulsion system. If this value is higher than 1, there is the beneficial mutual fit between propeller and AUV hull, in other words, it increases the overall efficiency of propulsion system. Fig. 17 shows the variation of hull efficiency, and it is noticeable that hull efficiency is lower than that in other cases when the angle of attack is 3°. For other angles of attack, the hull efficiency fluctuated between 1.20 and 1.32.

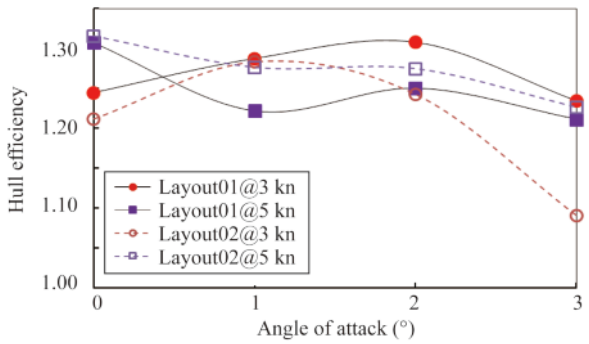

Fig. 17. Hull efficiency for different angles of attack.

6 Conclusions

The numerical and experimental study on self-propulsion of an autonomous underwater vehicle in deep water was presented in this paper. Simulations were carried out under constant depth conditions for different forward velocities and angles of attack without actuation on the control surfaces. The hull-propeller interaction of Explorer 1000 AUV for forward velocities from 2 kn to 5 kn was analyzed using a steady simulation method, in which a PID controller was designed to adjust propeller rotational velocity, so that a balance between propeller thrust and hull resistance can be reached. Good agreements with experimental results indicate that the developed approach is reliable while a large amount of computing time can be saved. We must acknowledge that some factors could not be taken into consideration, such as excitation force and unsteady vortex due to vibration of hull and adjustment of control surfaces. But we would also stress that our method is very time efficient, and is a suitable option for engineers and scientists to figure out self-propulsion point, thrust deduction, wake fraction and hull efficiency in a short period, which is highly beneficial to the design of underwater vehicles. Design can be optimized according to initial simulation results. When design is confirmed, further unsteady simulations can be carried out to better assess its overall performance.

For Explorer 1000, its average thrust deduction and wake fraction are 0.18 and 0.35, respectively, compared with most submarines whose average thrust deduction is between 0.10 and 0.18, and wake fraction between 0.10 and 0.25. It indicates that the hull-propeller interaction problem is serious and can be further improved. Our next steps will include optimization of hull-propeller interaction.

References

Bhattacharyya, A., Krasilnikov, V. and Steen, S., 2016. A CFD-based scaling approach for ducted propellers, *Ocean Engineering*, 123, 116–130.

Califano, A. and Steen, S., 2011. Numerical simulations of a fully submerged propeller subject to ventilation, *Ocean Engineering*, 38(14−15), 1582–1599.

Carrica, P.M., Castro, A.M. and Stern, F., 2010. Self-propulsion computations using a speed controller and a discretized propeller with dynamic overset grids, *Journal of Marine Science and Technology*, 15(4), 316–330.

Carrica, P.M., Kim, Y. and Martin, J.E., 2018. Near surface operation of a generic submarine in calm water and waves, *Proceedings of the 32nd Symposium on Naval Hydrodynamics*, *Hamburg*, *Germany*.

Chase, N. and Carrica, P.M., 2013. Submarine propeller computations and application to self-propulsion of DARPA Suboff, *Ocean Engineering*, 60, 68–80.

Coe, R.G., 2013. *Improved Underwater Vehicle Control and Maneuvering Analysis with Computational Fluid Dynamics Simulations*, Ph.D. Thesis, Virginia Polytechnic Institute and State University, Virginia.

De Barros, E. and Dantas, J.L.D., 2012. Effect of a propeller duct on AUV maneuverability, *Ocean Engineering*, 42, 61–70.

Denny, S.B., 1968. *Cavitation and Open-Water Performance Tests of A Series of Propellers Designed by Lifting-Surface Methods*, Department of the Navy Naval Ship Research and Development Center, Washington, D.C.

Di Felice, F., Felli, M., Liefvendahl, M. and Svennberg, U., 2009. Numerical and experimental analysis of the wake behavior of a generic submarine propeller, *First International Symposium Marine Propulsors*, Trondheim, Norway.

Dubbioso, G., Muscari, R. Ortolani, F. and Di Mascio, A., 2017. Analysis of propeller bearing loads by CFD. Part I: Straight ahead and steady turning maneuvers, *Ocean Engineering*, 130, 241–259.

Felli, M., Camussi, R. and Di Felice, F., 2011. Mechanisms of evolution of the propeller wake in the transition and far fields, *Journal of Fluid Mechanics*, 682, 5–53.

Gao, T., Wang, Y.X., Pang, Y.J. and Cao, J., 2016. Hull shape optimization for autonomous underwater vehicles using CFD, *Engineering Applications of Computational Fluid Mechanics*, 10(1), 599–607.

Gao, T., Wang, Y.X., Pang, Y.J., Chen, Q.L. and Tang, Y.G., 2018. A time-efficient CFD approach for hydrodynamic coefficient determ-

ination and model simplification of submarine, *Ocean Engineering*, 154, 16–26.

Gatchell, S., Hafermann, D. and Streckwall, H., 2011. Open water test propeller performance and cavitation behaviour using PPB and FreSCo, *Proceedings of the Second International Symposium Marine Propulsors*, Hamburg, Germany.

Guo, H.P., Zou, Z.J., Liu, Y. and Wang, F., 2018. Investigation on hull-propeller-rudder interaction by RANS simulation of captive model tests for a twin-screw ship, *Ocean Engineering*, 162, 259–273.

Hayati, A.N., Hashemi, S.M. and Shams, M., 2013. A study on the behind-hull performance of marine propellers astern autonomous underwater vehicles at diverse angles of attack, *Ocean Engineering*, 59, 152–163.

Hobson, B.W., Bellingham, J.G., Kieft, B., and Mcewen, R., Godin, M. and Zhang, Y.W., 2012. Tethys-class long range AUVs - extending the endurance of propeller-driven cruising AUVs from days to weeks, *IEEE/OES Autonomous Underwater Vehicles*, IEEE, Southampton, UK, pp. 1−8.

Kim, H., Ranmuthugala, D., Leong, Z.Q. and Chin, C., 2018. Six-DOF simulations of an underwater vehicle undergoing straight line and steady turning manoeuvres, *Ocean Engineering*, 150, 102–112.

Martínez-Calle, J., Balbona-Calvo, L., González-Pérez, J. and Blanco-Marigorta, E., 2002. An open water numerical model for a marine propeller: A comparison with experimental data, *ASME 2002 Joint U.S.-European Fluids Engineering Division Conference*, ASME, Montreal, Quebec, Canada.

Martio, J., Sánchez-Caja, A. and Siikonen, T., 2017. Open and ducted propeller virtual mass and damping coefficients by URANS-method in straight and oblique flow, *Ocean Engineering*, 130, 92–102.

Menter, F. R., 1994. Two-equation eddy-viscosity turbulence models for engineering applications, *AIAA Journal*, 32(8), 1598–1605.

Morgut, M. and Nobile, E., 2012. Influence of grid type and turbulence model on the numerical prediction of the flow around marine propellers working in uniform inflow, *Ocean Engineering*, 42, 26–34.

Overpelt, B., Nienhuis, B. and Anderson, B., 2015. Free running manoeuvring model tests on a modern generic SSK class submarine (BB2), *Proceedings of Pacific 2015*, Sydney, Australia.

Phillips, A.B., Turnock, S.R. and Furlong, M., 2009. Evaluation of manoeuvring coefficients of a self-propelled ship using a blade element momentum propeller model coupled to a Reynolds-averaged Navier−Stokes flow solver, *Ocean Engineering*, 36(15−16), 1217–1225.

Phillips, A.B., 2010. *Simulations of A Self Propelled Autonomous Underwater Vehicle*, Ph. D. Thesis, University of Southampton, Southampton.

Phillips, A.B., Turnock, S.R. and Furlong, M., 2010. Influence of turbulence closure models on the vortical flow field around a submarine body undergoing steady drift, *Journal of Marine Science and Technology*, 15(3), 201–217.

Rhee, S.H. and Joshi, S., 2005. Computational validation for flow around a marine propeller using unstructured mesh based navier-stokes solver, *JSME International Journal Series B*: *Fluids and Thermal Engineering*, 48(3), 562–570.

Sezen, S., Dogrul, A., Delen, C. and Bal, S., 2018. Investigation of self-propulsion of DARPA Suboff by RANS method, *Ocean Engineering*, 150, 258–271.

Shen, H.L., Obwogi, E.O. and Su, Y., 2016. Scale effects for rudder bulb and rudder thrust fin on propulsive efficiency based on computational fluid dynamics, *Ocean Engineering*, 117, 199–209.

Shen, Z.R., Wan, D.C. and Carrica, P.M., 2015. Dynamic overset grids in OpenFOAM with application to KCS self-propulsion and maneuvering, *Ocean Engineering*, 108, 287–306.

Stern, F., Wang, Z.Y., Yang, J.M., Sadat-Hosseini, H., Mousaviraad, M., Bhushan, S., Diez, M., Yoon, S.H., Wu, P.C., Yeon, S.M., Dogan, T., Kim, D.H., Volpi, S., Conger, M., Michael, T., Xing, T., Thodal, R.S. and Grenestedt, J.L., 2015. Recent progress in CFD for naval architecture and ocean engineering, *Journal of Hydrodynamics*, *Ser. B*, 27(1), 1–23.

Ueno, M. and Tsukada, Y., 2016. Estimation of full-scale propeller torque and thrust using free-running model ship in waves, *Ocean Engineering*, 120, 30–39.

Wang, J.H., Zou, L. and Wan, D.C., 2018. Numerical simulations of zigzag maneuver of free running ship in waves by RANS-Overset grid method, *Ocean Engineering*, 162, 55–79.

Wang, Y.X., Gao, T., Pang, Y.J. and Tang, Y.G., 2019. Investigation and optimization of appendage influence on the hydrodynamic performance of AUVs, *Journal of Marine Science and Technology*, 24(1), 297–305.

Young, Y.L. and Kinnas, S.A., 2003. Analysis of supercavitating and surface-piercing propeller flows via BEM, *Computational Mechanics*, 32(4−6), 269–280.